Received: 16 May 2022 | Revised: 22 June 2022 | Accepted: 24 June 2022

DOI: 10.1002/jbio.202200151

RESEARCH ARTICLE

JOURNAL OF BIOPHOTONICS

Label-free detection of cardiac troponin-I with packaged thin-walled microbubble resonators

Zhihe Guo[1] | Xuyang Zhao[1] | Yi Zhou[1] | Yuxiang Li[1] | Zhiran Liu[1] | Man Luo[1] | Xiang Wu[1*] | You Wang[2] | Meng Zhang[2] | Xi Yang[2]

[1]Department of Optical Science and Engineering, Shanghai Engineering Research Center of Ultra Precision Optical Manufacturing, Fudan University, Shanghai, China

[2]Key Laboratory of Laser Device Technology, China North Industries Group Corporation Limited, Southwest Institute of Technical Physics, Chengdu, China

***Correspondence**
Xiang Wu, Department of Optical Science and Engineering, Shanghai Engineering Research Center of Ultra Precision Optical Manufacturing, Fudan University, Shanghai 200433, China.
Email: wuxiang@fudan.edu.cn

Funding information
National Natural Science Foundation of China, Grant/Award Number: 62175035; Natural Science Foundation of Shanghai, Grant/Award Number: 21ZR1407400; Open-Foundation of Key Laboratory of Laser Device Technology, China North Industries Group Corporation Limited, Grant/Award Number: KLLDT202108

Abstract

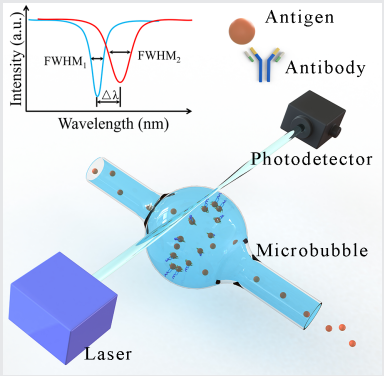

The measurement of cardiac troponin-I (cTnI) is widely used for diagnosing acute myocardial infarction (AMI) diseases because of its myocardial specificity. Packaged microbubble resonators with thin wall are utilized for label-free and specific detection of cTnI based on whispering gallery mode (WGM). This packaged structure can provide a good protection for the biosensor, improve the anti-interference ability of the sensor and reduce the system noise. The theoretical detection limit of the biosensors for cTnI in phosphate buffer saline (PBS) is 0.4 ag mL^{-1} (0.02 a_M). Furthermore, we demonstrated that the biosensors can be used to detect cTnI molecules in simulated serum and the theoretical detection limit is also 0.4 ag mL^{-1} (0.02 a_M). These results are much far below the clinical cut-off value and show a huge application potential for the detection of cardiac biomarkers of AMI.

KEYWORDS
label-free biosensors, microbubble resonators, whispering gallery modes

1 | INTRODUCTION

Early diagnosis of acute myocardial infarction (AMI), via high-sensitive detection of its specific biomarker, can effectively treat the disease and significantly reduce the mortality rate [1, 2]. Troponin is a regulatory protein of the thin filament of striated muscle, released into the bloodstream 4 to 6 hours after AMI and the peak levels occur at 18 to 24 hours [3]. Assessment of troponin is a sensitive and specific method for diagnosing AMI. Among the biomarkers of AMI, the clinical sensitivity and specificity of cardiac troponin I (cTnI) have been reported to 90.7% and 90.2%, respectively [4, 5]. CTnI is widely used as the gold standard for the diagnosis of AMI and the clinical cut-off value of cTnI is recommended of <0.1 ng mL^{-1} [3, 4, 6–8]. Therefore, it is a matter of great urgency to establish a sensing system with high sensitivity and rapid detection of cTnI concentration in real time to provide

Abbreviations: AMI, acute myocardial infarction; BSA, bovine serum albumin; cTnI, cardiac troponin-I; DL, detection limit; FEM, finite element method; GOPTS, 3-glycidoxypropyltrimethoxysilan; HD, hyperboloid-drum; HF, hydrofluoric acid; IgG, immunoglobulin G; MSD, molecular surface density; PBS, phosphate buffer saline; PSA, prostate-specific antigen; Q, quality factor; S, sensitivity; SEM, scanning electron microscope; WGM, whispering gallery modes.

Zhihe Guo and Xuyang Zhao have contributed equally to this work.

prognostic information supporting risk stratification and highly accurate diagnostics at the early stage [2, 9].

Various highly sensitive biosensors and biosensing techniques have been continually proposed and evolving to enhance analytical performance for target biomarkers [2, 10, 11]. Foreign labeling or tracer agents, such as isotope, enzymes, metal nanoparticles and fluorescent materials, are developed to generate or amplify the weak sensing signal [2]. However, it requires a labeling process as a preparation step that is usually low yield, combining synthesis and purification [12]. Some tracers even require a long incubation process and fluorescent materials have bleaching effects. Label-free sensing technique does not need any other foreign compound for detection, can alleviate some of the practical limitations of labeled sensors. The main advantage for label-free detection is that more information can be acquired directly, as the methods use only native proteins and ligands [12, 13].

Whispering gallery mode (WGM) microcavity resonator has been exploited for a broad field of fundamental research and practical applications in recent years benefits by their high quality (Q) factor and small mode volume, which can be used as one of the label-free biosensors [14–17]. The detection limits (DLs) of some WGM biosensors such as microtoroid and microbubble have reached to several aM or even to single-molecule level [18, 19]. A label-free hyperboloid-drum (HD) microdisk laser, fabricated from a silica microdisk coated with the gain medium, represents a biosensing capabilities of human IgG with a theoretical DL of 9 ag mL^{-1} [20]. In particular, the hollow structure of microbubble can be used as a natural microfluidic channel, which is convenient for the fabrication of integrated sensor devices. Microbubbles have been widely used in various biochemical sensing experiments [21–26].

We present an ultrasensitive biosensor using thin-walled microbubble resonators. With the help of packaged method, the coupling position between the microbubble and the fiber taper is fixed. It can aid to eliminate the noise from surrounding environments and improve the stability of the resonator. Furthermore, the thin-walled structure is helpful for the light field to enter the analyte, enhancing the interaction strength between light and matter, and improve the sensitivity. The microbubble resonator is applied to specific detection of cTnI in phosphate buffer saline (PBS) and simulated serum.

2 | MATERIALS AND METHODS

2.1 | Materials and reagents

The microbubble was fabricated from a fused silica capillary (TSP075150, Zhengzhou INNOSEP Scientific, China). The low refractive index UV glue (MY-133-V2000, $n = 1.33$) was purchased from MY Polymers Ltd., Israel. 3-Glycidoxypropyltrimethoxysilan (GOPTS) was purchased from Aladdin, China. Bovine serum albumin (BSA) and PBS (diluted to 1×) were purchased from Sigma Aldrich. Anti-cTnI and cTnI (24 kDa) were obtained from Shanghai Linc-Bio Science (Shanghai, China). Human immunoglobulin G (IgG) was obtained from Dingguo Changsheng Biotechnology (Beijing, China). Prostate-specific antigen (PSA) protein was purchased from Cholun Medical (Shenzhen, China). Simulated serum was purchased from InnoReagents (Huzhou, China). All reagents were directly used without further purification.

GOPTS is mixed with ethanol in 1% volume ratio and used for silanization of the microbubble inner surfaces. The anti-cTnI antibody and BSA were prepared using PBS with a concentration of 0.5 mg mL^{-1}, respectively. CTnI protein was diluted with PBS to 1, 10 and 100 ag mL^{-1}; 1, 10 and 100 fg mL^{-1}; 1, 10 and 100 pg mL^{-1}; and 1, 10 and 100 ng mL^{-1}. CTnI protein was also diluted with simulated serum with the concentrations ranged from 1 ag mL^{-1} to 100 ng mL^{-1}.

2.2 | Fabrication processes and experimental setup

In order to improve the anti-interference ability of the sensor and reduce the system noise, the microbubble and the fiber taper are wrapped with MY-133-V2000 to form a packaged sample. The fabrication processes of the packaged microbubble resonator are similar to Refs [17, 27] and the schematic diagram of the sensor is shown in Figure 1A. First, fix the fiber taper on the glass scaffold with UV glue. Next, the fiber taper is coupled with the microbubble by using 5D optic alignment stages. The capillaries on both sides of the microbubble are fixed on the glass scaffold to reduce the change of coupling position. After that, the optical coupling region between the fiber taper and the microbubble is completely wrapped with MY-133-V2000 to further improve the stability of the sensor. Finally, place a coverslip over the glass scaffold to form a sealed environment, so that MY-133-V2000 can be isolated from oxygen and accelerate its curing. The diameter of the microbubble is approximately 296 μm. It is coupled with a fiber taper to realize the light input and output, as shown in Figure 1B. The influence of scattering and absorption loss caused by the UV glue (MY-133-V2000) is insignificant, which is estimated by the measurement of Q-factor before and after the packaging process [27, 28]. Therefore, the packaging process has insignificant influence on the sensing performance of microbubble biosensors.

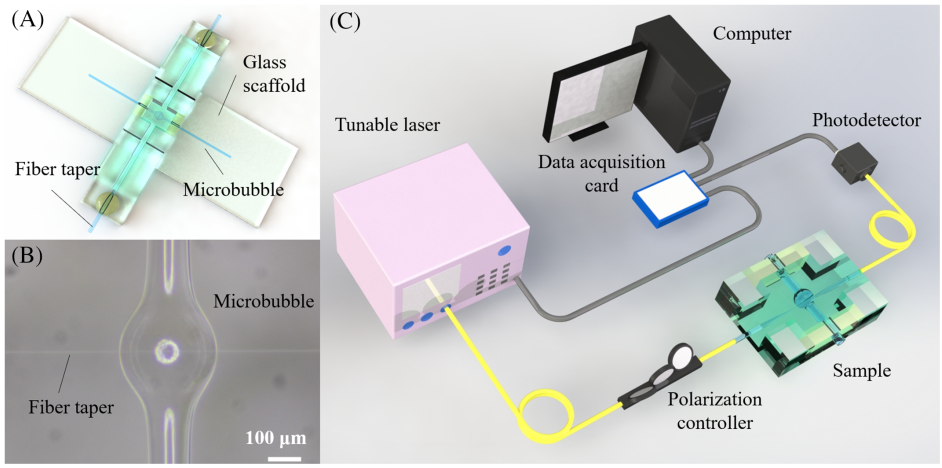

FIGURE 1 (A) Schematic diagram of the packaged microbubble resonator. (B) Microscope image of a fiber taper and a microbubble. (C) Experimental setup of packaged microbubble biosensor

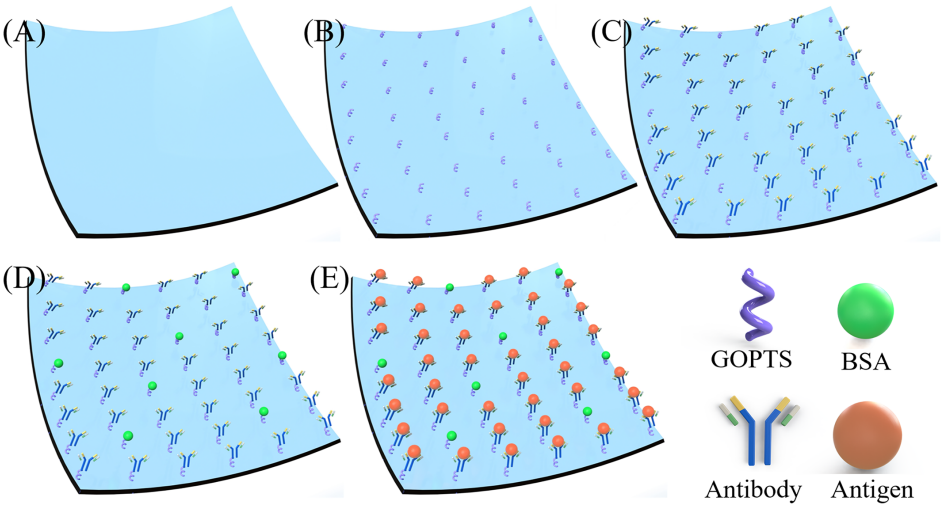

FIGURE 2 Surface functionalization processes for specific detection of cTnI. (A) and (B) are the surface silylanization processes of the biosensor. (C) Antibody binds to GOPTS. (D) Using BSA to block the unbound sites. (E) Detection of antigen cTnI

The experimental setup is shown in Figure 1C. The tunable laser (780 nm, UniQuanta, China) is coupled into the fiber and collected by a photodetector (PDA36A2, Thorlabs). The polarization state of light from the tunable laser is adjusted by the polarization controller. The optical signals from the photodetector are recorded by the data acquisition card (PCIe 6351, National Instruments). Since WGM sensor is very sensitive to environmental conditions (such as temperature), it is necessary to keep the temperature around the sensor constant during the experiment. Therefore, all the experiments are performed in the indoor environment unless otherwise noted (22°C room temperature and 40% humidity).

Normally, biomolecular binding can induce the change of the local refractive index at the inner surface of the microbubble, resulting in the shift of the transmission spectrum. The sensitivity of the sensor is related to the surface density of biomolecules and the intensity of evanescent-field. In order to capture biomarkers specifically, the sensor surface needs to be functionalized.

2.3 | Functionalization of biosensor surface

The immobilization of proteins on the packaged microbubble inner surface and the biodetection processes are shown in Figure 2. The ethanol solution containing 1% GOPTS was extracted into the microbubbles and incubated for 2 hours to silylate the inner surface. Then, the inner surface of the microbubble was washed with distilled water and ethanol solution. Thirdly, the microbubble was heated at 120°C for 2 hours. Afterward, the microbubble was fabricated into the packaged microbubble resonator [22, 27–29].

Before the cTnI antigen detection, the anti-cTnI antibody modification in microbubble inner surface is required. Firstly, the anti-cTnI antibody (500 μg mL^{-1}) was extracted into the packaged microbubble resonator through the syringe pump for 2 hours as shown in Figure 2C. During the modification process, the flow rate of the solution was set as 3 μL min^{-1}. Then replace the antibody solution with PBS solution to wash the inner

surface. To reduce subsequent non-specific binding, BSA solution (500 μg mL^{-1}) was then performed for 0.5 hour, as shown in Figure 2D. The packaged microbubble biosensor was then washed with PBS for 5 minutes. Finally, the various concentrations of cTnI solutions, diluted with PBS and simulated serum, were detected with this biosensing system, as shown in Figure 2E.

3 | RESULTS AND DISCUSSION

3.1 | Optical mode analysis

Normally, the refractive index changing of solution or biomolecular bindings can change the local refractive index at the microbubble interior, inducing the shift of the transmission spectrum. The sensitivity (S) of a sensor is related to the intensity of the interaction between light and matter. The relation between the S and the distribution fraction of the light energy in the liquid (η) can be expressed as [30]:

$$S = \frac{\delta\lambda}{\delta n} \approx \frac{\lambda}{n_1}\eta, \tag{1}$$

where δn represents the refractive index change of the liquid; n_1 is the refractive index of the microbubble; $\delta\lambda$ is the wavelength shift in resonant wavelength (λ). η can be written as [30]:

$$\eta \cong \frac{n^2 Rh\lambda |E_0|^2}{2\varepsilon_{rs}\sqrt{n_1^2 - n^2}\int |E|^2 dV}, \tag{2}$$

where n is the refractive index of the liquid; R is the radius of the microbubble; h is an arbitrary length along the resonator longitudinal direction; $\varepsilon_s = \varepsilon_0\varepsilon_{rs}$ is the dielectric constant of the resonator; E_0 represents the electric field amplitude in the liquid; E represents the electric field amplitude of a WGM throughout the resonator. The integral in the denominator of Equation (2) is taken over the volume (V) of the WGM. In the same microcavity, the λ, E_0 and E of different WGMs will be different. For the convenience of analysis, we expressed the changes of λ, E_0 and E with η_0, which was written as:

$$\eta_0 = \frac{\lambda |E_0|^2}{\int |E|^2 dV}. \tag{3}$$

Therefore, Equation (2) can be written as:

$$\eta \cong \frac{n^2 Rh}{2\varepsilon_{rs}\sqrt{n_1^2 - n^2}}\eta_0. \tag{4}$$

Equation (4) indicates that η is linearly proportional to η_0. Increasing of the electric field distribution in the liquid (E_0) can obtain a greater η and S.

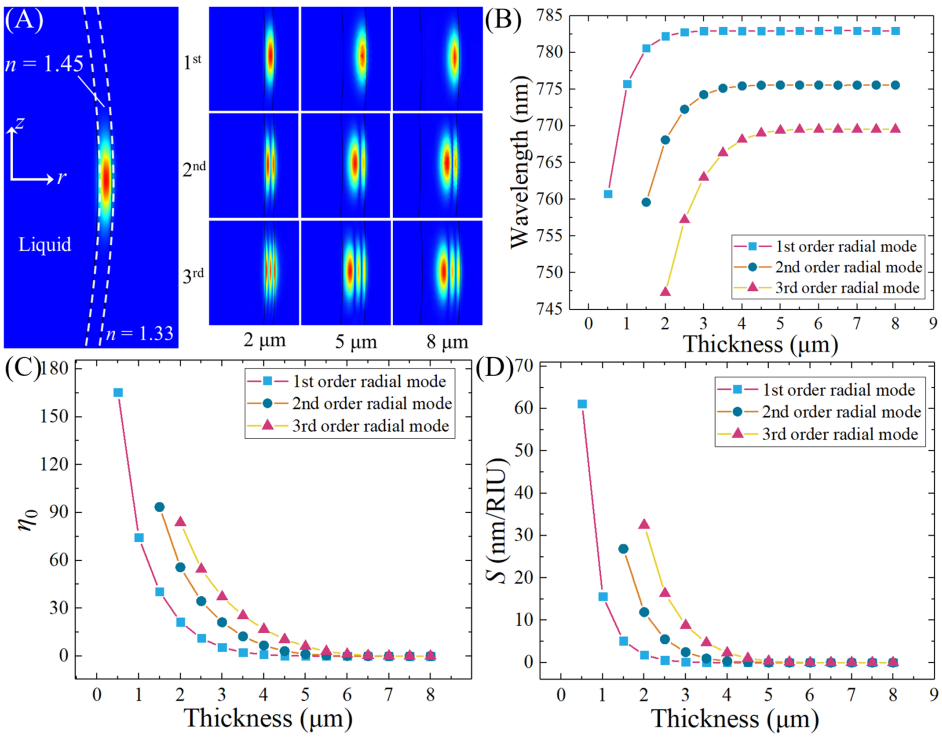

FIGURE 3 (A) Field distributions of WGMs in different-order-radial mode with 2, 5 and 8 μm wall thickness. Results of FEM for (B) resonant wavelength (λ), (C) η_0 and (D) refractive index sensitivity (S) in different-order-radial mode at different wall thicknesses, respectively

Figure 3 exhibits the numerical simulations based on the finite element method (FEM, by COMSOL Multiphysics). The influences of the wall thickness and different-order radial WGM of the microbubble to the sensitivity were investigated. The field distributions of WGMs in different-order-radial mode with 2, 5 and 8 μm wall thickness were shown in Figure 2A. For the same radial-order of WGMs, the increase of wall thickness will lead to the decrease of η_0 while the increase of the resonant wavelength (λ), as shown in Figure 3B,C, respectively. Therefore, S decreases gradually as the wall thickness increases. Thicker wall thickness will lead to more light fields confined inside the silica wall, only a few fractions of light fields can leak into the interior of the microbubble which will interact with the matter, resulting in a low sensitivity. These simulations indicated that selecting a microbubble with a thinner wall thickness is able to obtain a greater η_0, enhance the interaction strength between light and matter, which can aid in achieving a higher sensitivity and a lower DL. However, the microbubbles are too fragile and difficult to fabricate the packaged resonators once the wall thickness of the microbubble is thinner than 1 μm. Especially, it is difficult to form a sufficient confinement of WGMs when the outside of the microbubble is wrapped by MY-133-V2000. Therefore, in order to form the sufficient confinement of WGMs while obtain high sensitivity, the compromise scheme is to select microbubbles with wall thickness ranging from 1 to 3 μm.

Firstly, hydrofluoric acid (HF) was extracted at a uniform speed (20 μL mL^{-1}) by the syringe pump to corrode the inner wall of the silica capillary and reduce the wall thickness to 7-9 μm. Then, deionized water was extracted to clean the residual HF inside the inner silica capillary. Finally, extract clean air to dry the inner wall of the microtubule. The thinned silica capillary can be used to fabricate the thin-walled microbubbles. In order to accurately measure its sizes, we twisted the microbubbles and observed their cross-section under scanning electron microscope (SEM). The microbubble with a diameter of ~256 μm and a wall thickness of ~1.7 μm was shown in Figure 4.

3.2 | Detection of CtnI

The WGM spectrum of typical microbubble resonator was shown in Figure 5A. With Lorentz linear fitting, its Q factor was approximately 1.5×10^5. During the term of ~3600 s, the SD of center wavelength of WGM was 0.11 pm, as shown in Figure 5B. It shows that the system has good stability and meets the subsequent sensing and detection requirements.

Before the detection of biomolecules, we test the bulk refractive index sensitivity of different WGM modes (wavelengths) with dimethyl sulfoxide solutions to find a high-sensitivity mode. The surface functionalization of the microbubble was illustrated in Figure 2; each sample was sequentially extracted into the biosensor at a flow rate of 3 μL min^{-1} for 10 min. The sample containing cTnI bound with the antibody were measured as the change in resonant wavelength. Figure 5C is the wavelength responses of sensing cTnI in PBS. Each error bar in Figure 5C represents the SD from three independent measurements by using the same biosensor (including the functionalization procedures).

Moreover, there is a linear relationship between the wavelength shift of WGM and the molecular surface density (MSD, molecules cm^{-2}) on the inner surface of the microbubble, which provides a quantitative analysis method for detecting molecules [30]:

$$\mathrm{MSD} = \frac{1}{\alpha_{\mathrm{ex}}} \frac{n^2}{n_1} \frac{\varepsilon_0 \lambda}{2\pi\sqrt{n_1^2 - n^2}} \frac{\delta\lambda}{S}, \tag{5}$$

where α_{ex} (cm^3) is the excess polarizability of the analyte. For antibody (anti-cTnI) and BSA, the values can be

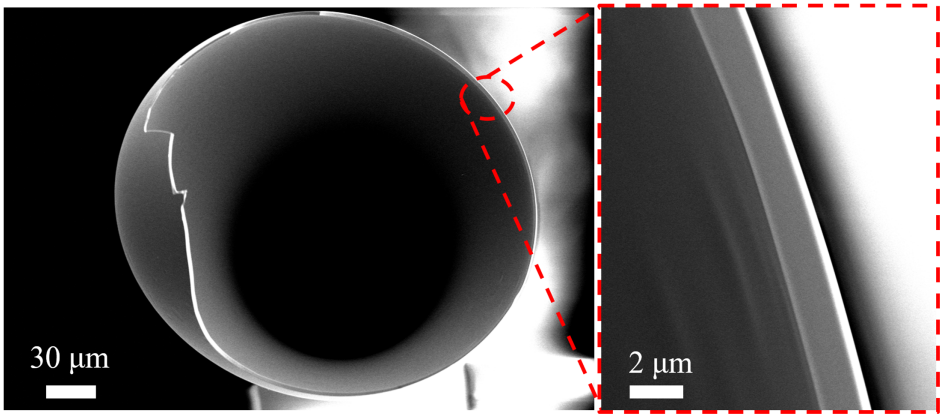

FIGURE 4 SEM images of a microbubble. Its diameter and wall thickness were ~256 and ~1.7 μm, respectively

determined to be $4\pi\varepsilon_0$ (8.7×10^{-21}) cm^3 and $4\pi\varepsilon_0$ (3.85×10^{-21}) cm^3, respectively. The wavelength shifts caused by antibody and BSA were approximately 17.2 and 1.2 pm, respectively. The bulk refractive index sensitivity of the microbubble sensor was $S = 6.3$ nm/RIU. By using Equation (5), the theoretical MSDs of antibody and BSA were calculated as 4.1×10^{12} and 2.8×10^{11} molecules cm^{-2}, respectively. The SD of blank sample is approximately $\sigma = 0.11$ pm, and the sensitivity of the linear variation region is $S_1 = 0.8$ pm mL ag^{-1}. Therefore, the theoretical detection limit can be estimated as DL $= 3\sigma/S_1 = 0.4$ ag mL^{-1} (0.02 a_M).

In order to promote clinical application and verify the feasibility of the sensor for specific detection of biomolecules in complex environments, we demonstrated the feasibility of the microbubble sensor for specific detection of cTnI in a simulated serum. CTnI was diluted with the simulated serum into different concentrations. After processing according to the same surface functionalization process shown in Figure 2, the optical response to different concentrations of simulated serum samples was measured. Figure 5D exhibited the results of the simulated serum samples at concentrations ranged from 1 ag mL^{-1} to 100 ng mL^{-1}. These responses are almost identical to that for cTnI in PBS. The sensitivity of the linear variation region is $S_2 = 0.9$ pm mL ag^{-1}, and the theoretical DL can be estimated as DL $= 3\sigma/S_2 = 0.4$ ag mL^{-1} (0.02 a_M).

Table 1 summarizes a series of various biosensing technologies for cTnI that have been reported in recent years [31–36]. Compared with the existing and emerging biosensors, the packaged thin-walled microbubble biosensor has a lager measure range and lower DL of cTnI. The results of the biosensors are approximately four orders of magnitude more sensitive than these biosensors.

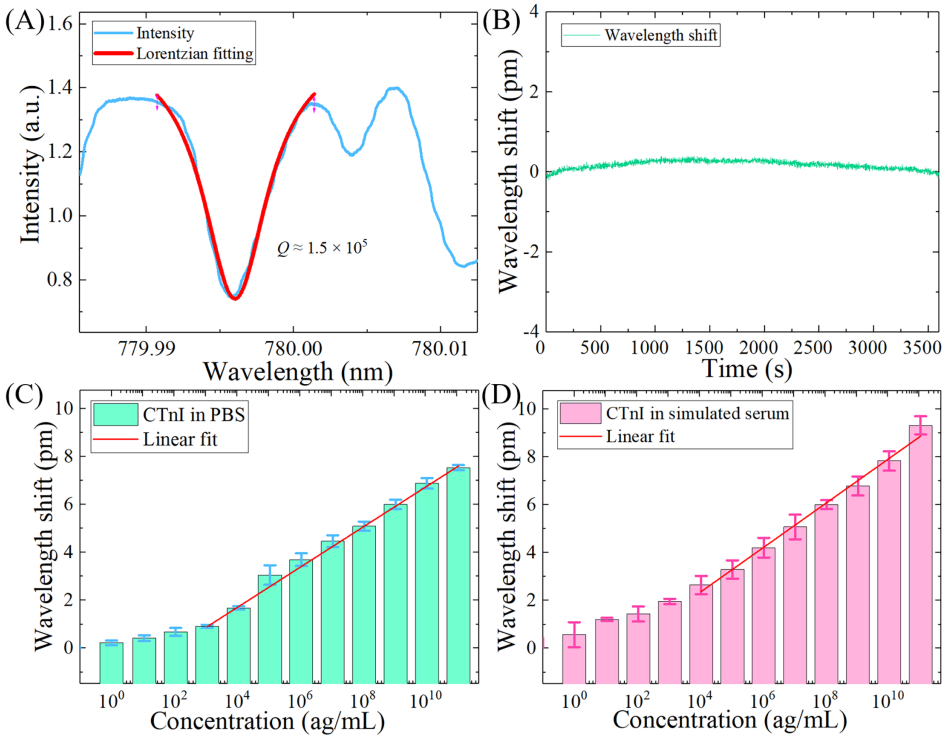

FIGURE 5 (A) Transmission spectrum of packaged microbubble resonator. (B) Wavelength shift of the resonator during a period of ~3600 s. (C) and (D) are the measured response as a function of cTnI concentrations in PBS and simulated serum, respectively

TABLE 1 Comparisons of different biosensors for the detection of cTnI

Platform	Analyte	Measure range	Detection limit	Ref
Microsphere	cTnI-C	0.3 to 2.0 ng mL^{-1}	0.59 ng mL^{-1}	[31]
SERS	cTnI	0 to 2.0 ng mL^{-1}	9.80 pg mL^{-1}	[32]
Plasmon	cTnI	—	0.015 ng mL^{-1}	[33]
Microfiber	cTnI	2 to 10 fg mL^{-1}	2 fg mL^{-1}	[34]
ELISA	cTnI	1 pg mL^{-1} to 1 ng mL^{-1}	0.31 pg mL^{-1}	[35]
Voltammetry	cTnI	0.01 to 5.00 ng mL^{-1}	0.0005 ng mL^{-1}	[36]
Microbubble	cTnI	1 ag mL^{-1} to 100 ng mL^{-1}	0.5 ag mL^{-1}	This work

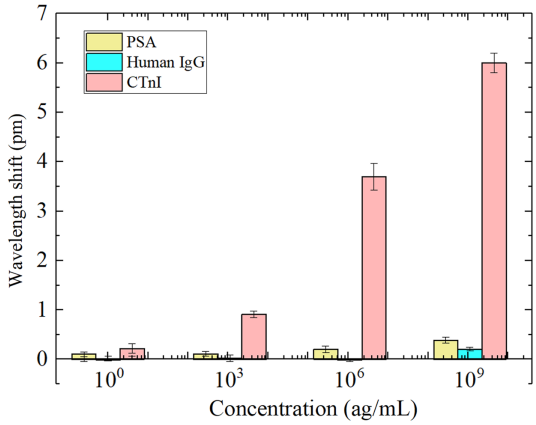

FIGURE 6 Measured wavelength responses comparisons between cTnI antigen and other non-specific protein (PSA, human IgG) with the concentration of 1 ag mL^{-1}, 1 fg mL^{-1}, 1 pg mL^{-1} and 1 ng mL^{-1} in PBS buffer

3.3 | Specificity test

The specificity test of the packaged microbubble biosensor for cTnI was checked in presence of human IgG and PSA in PBS, as shown in Figure 6. The concentrations of human IgG, PSA and cTnI were set as 1 ag mL^{-1}, 1 fg mL^{-1}, 1 pg mL^{-1} and 1 ng mL^{-1}. After the sensor surface was immobilized with anti-cTnI antibody and blocked with BSA, these different concentrations of solutions were separately extracted into the packaged microbubble biosensor. As shown in Figure 6, the result indicates that the wavelength shift induced by target cTnI protein is larger than other proteins. The stronger response suggests good specificity of the packaged microbubble biosensor for cTnI protein detection.

4 | CONCLUSION

The specific detection of cTnI was realized by using a packaged microbubble resonator. Benefit for its thin-walled structure, the analyte cTnI can interact strongly with the light field in the inner surface of microbubble. The theoretical DL of the microbubble biosensors for cTnI is 0.4 ag mL^{-1} (0.02 a_M) in PBS. Furthermore, we demonstrated that the biosensors can be used to detect cTnI molecules in simulated serum and the theoretical DL is also 0.4 ag mL^{-1} (0.02 a_M). The results of the biosensors were approximately four orders of magnitude more sensitive than the existing and emerging biosensors for the detection of cTnI. It can be predicted that optical thin-walled microbubble biosensor is expected to become a candidate for the point-of-care devices, which can provide a feasible scheme for reliable precision detection or dynamic monitoring of life-threatening disease biomarkers (such as cTnI and cTnT of AMI).

AUTHOR CONTRIBUTIONS

The research was conducted by Zhihe Guo and Xuyang Zhao at Fudan University. The research was conceptualized by Zhihe Guo, Xiang Wu and Yi Zhou. The participant interaction and experimental procedures (data acquisition, processing and analysis) were carried out by Zhihe Guo, Xuyang Zhao and Xiang Wu. This research article was drafted by Zhihe Guo, with input and assistance from the remaining other authors. All the authors have read this article before submission for peer review. All the authors have accepted responsibility for the entire content of this submitted manuscript and approved submission.

ACKNOWLEDGMENTS

The work was supported by the Natural Science Foundation of Shanghai (21ZR1407400), National Natural Science Foundation of China (62175035) and Open-Foundation of Key Laboratory of Laser Device Technology, China North Industries Group Corporation Limited (KLLDT202108).

CONFLICT OF INTEREST

The authors declare no financial or commercial conflict of interest.

DATA AVAILABILITY STATEMENT

The data that support the findings of this study are available from the corresponding author upon reasonable request.

ORCID

Zhihe Guo https://orcid.org/0000-0001-5439-2829
Xiang Wu https://orcid.org/0000-0001-7936-2271

REFERENCES

[1] K. Thygesen, J. S. Alpert, A. S. Jaffe, B. R. Chaitman, J. J. Bax, D. A. Morrow, H. D. White, Executive Group, *J. Am. Coll. Cardiol.* **2018**, *72*, 2231.
[2] D. H. Kim, W. Chegal, Y. J. Cho, L. Van Le, M. S. Diware, S.-H. Paek, Y. D. Kim, H. M. Cho, *Biosens. Bioelectron.* **2020**, *168*, 112525.
[3] L. H. Madsen, G. Christensen, T. Lund, V. L. Serebruany, C. B. Granger, I. Hoen, Z. Grieg, J. H. Alexander, A. S. Jaffe, J. E. Van Eyk, D. Atar, *Circ. Res.* **2006**, *99*, 1141.
[4] T. Keller, T. Zeller, D. Peetz, S. Tzikas, A. Roth, E. Czyz, C. Bickel, S. Baldus, A. Warnholtz, M. Fröhlich, C. R. Sinning, M. S. Eleftheriadis, P. S. Wild, R. B. Schnabel, E. Lubos, N. Jachmann, S. Genth-Zotz, F. Post, V. Nicaud, L. Tiret, K. J. Lackner, T. F. Münzel, S. Blankenberg, *N. Engl. J. Med.* **2009**, *361*, 868.

[5] H. Zhao, Q. Lin, L. Huang, Y. Zhai, Y. Liu, Y. Deng, E. Su, N. He, *Nanoscale* **2021**, *13*, 3275.
[6] M. W. Sherwood, L. Kristin Newby, *J. Am. Hear. Assoc.* **2014**, *3*, e000403.
[7] A. Periyakaruppan, R. P. Gandhiraman, M. Meyyappan, J. E. Koehne, *Anal. Chem.* **2013**, *85*, 3858.
[8] A. Pourali, M. R. Rashidi, J. Barar, G. Pavon-Djavid, Y. Omidi, *TrAC Trends Anal. Chem.* **2021**, *134*, 116123.
[9] D. A. Morrow, E. M. Antman, M. Tanasijevic, N. Rifai, J. A. de Lemos, C. H. McCabe, C. P. Cannon, E. Braunwald, *J. Am. Coll. Cardiol.* **2000**, *36*, 1812.
[10] Y. Wang, S. Zeng, G. Humbert, H.-P. Ho, *Laser Photonics Rev.* **2020**, *14*, 2000135.
[11] Y. Shi, Z. Li, P. Y. Liu, B. T. T. Nguyen, W. Wu, Q. Zhao, L. K. Chin, M. Wei, P. H. Yap, X. Zhou, H. Zhao, D. Yu, D. P. Tsai, A. Q. Liu, *Adv. Photonics Res.* **2021**, *2*, 2000150.
[12] A. Syahir, K. Usui, K.-Y. Tomizaki, K. Kajikawa, H. Mihara, *Microarrays* **2015**, *4*, 228.
[13] Y. Liu, H. Zhou, Z. Hu, G. Yu, D. Yang, J. Zhao, *Biosens. Bioelectron.* **2017**, *94*, 131.
[14] D. Yu, M. Humar, K. Meserve, R. C. Bailey, S. N. Chormaic, F. Vollmer, *Nat. Rev. Methods Primers* **2021**, *1*, 1.
[15] L. Cai, J. Pan, Y. Zhao, J. Wang, S. Xiao, *Phys. Status Solidi A* **2020**, *217*, 1900825.
[16] X. Yang, C. Gong, C. Zhang, Y. Wang, G.-F. Yan, L. Wei, Y.-C. Chen, Y.-J. Rao, Y. Gong, *Laser Photonics Rev.* **2022**, *16*, 2270004.
[17] X. Zhao, Z. Guo, Y. Zhou, J. Guo, Z. Liu, Y. Li, M. Luo, X. Wu, *Micromachines* **2022**, *13*, 592.
[18] E. Ozgur, K. E. Roberts, E. O. Ozgur, A. N. Gin, J. R. Bankhead, Z. Wang, J. Su, *Anal. Chem.* **2019**, *91*, 11872.
[19] X.-C. Yu, S.-J. Tang, W. Liu, Y. Xu, Q. Gong, Y.-L. Chen, Y.-F. Xiao, *Proc. Natl. Acad. Sci.* **2022**, *119*, e2108678119.
[20] Z. Guo, Y. Qin, P. Chen, J. Hu, Y. Zhou, X. Zhao, Z. Liu, Y. Fei, X. Jiang, X. Wu, *Small* **2020**, *16*, 2000239.
[21] M. Li, X. Wu, L. Liu, X. Fan, L. Xu, *Anal. Chem.* **2013**, *85*, 9328.
[22] Z. Guo, Q. Lu, C. Zhu, B. Wang, Y. Zhou, X. Wu, *Opt. Express* **2019**, *27*, 12424.
[23] L. Fu, Q. Lu, X. Liu, X. Chen, X. Wu, S. Xie, *Talanta* **2020**, *213*, 120815.
[24] Z. Wang, Y. Liu, H. Wang, S. Wang, K. Liu, T. Xu, J. Jiang, Y.-C. Chen, T. Liu, *Sens. Actuators B* **2022**, *359*, 131608.
[25] Z. Wang, Y. Liu, C. Gong, Z. Yuan, L. Shen, P. Chang, K. Liu, T. Xu, J. Jiang, Y.-C. Chen, T. Liu, *PhotoniX* **2021**, *2*, 1.
[26] X. Zhao, Y. Chen, Z. Guo, Y. Zhou, J. Guo, Z. Liu, X. Zhang, L. Xiao, Y. Fei, X. Wu, *Opt. Express* **2022**, *30*, 8317.
[27] T. Tang, X. Wu, L. Liu, L. Xu, *Appl. Optics* **2016**, *55*, 395.
[28] Z. Li, C. Zhu, Z. Guo, B. Wang, X. Wu, Y. Fei, *Micromachines* **2018**, *9*, 274.
[29] Z. Chen, Z. Guo, X. Mu, Q. Li, X. Wu, H. Fu, *Opt. Express* **2019**, *27*, 36932.
[30] H. Zhu, I. M. White, J. D. Suter, P. S. Dale, X. Fan, *Opt. Express* **2007**, *15*, 9139.
[31] P. Niu, J. Jiang, K. Liu, S. Wang, J. Jing, T. Xu, T. Wang, Y. Liu, T. Liu, *Biosens. Bioelectron.* **2022**, *208*, 114238.
[32] C. Hu, L. Ma, F. Mi, M. Guan, C. Guo, F. Peng, S. Sun, X. Wang, T. Liu, J. Li, *New J. Chem.* **2021**, *45*, 3088.
[33] X. Han, H. S. Kojori, R. M. Leblanc, S. J. Kim, *Anal. Chem.* **2018**, *90*, 7795.
[34] W. Zhou, K. Li, Y. Wei, P. Hao, M. Chi, Y. Liu, Y. Wu, *Biosens. Bioelectron.* **2018**, *106*, 99.
[35] X. Tan, L. Zhang, Q. Tang, G. Zheng, H. Li, *Microchim. Acta* **2019**, *186*, 1.
[36] M. L. Yola, N. Atar, *Biosens. Bioelectron.* **2019**, *126*, 418.

How to cite this article: Z. Guo, X. Zhao, Y. Zhou, Y. Li, Z. Liu, M. Luo, X. Wu, Y. Wang, M. Zhang, X. Yang, *J. Biophotonics* **2022**, *15*(10), e202200151. https://doi.org/10.1002/jbio.202200151